A Multichannel Array-Driven Scanner With Low Thermal EMF

Lushuai Qian, Yaqiong Fu, Zhengkun Li, Cunkai Zhang, and Le Chen

***Abstract*— In this paper, a multichannel array-driven scanner with low thermal electromotive force (EMF) is proposed for precision electrical measurement. Three novel approaches are adopted to decrease the thermal EMF of the scanner and improve its stability. An array-type control and detection system is proposed to realize the closed-loop control of the relays, which can effectively simplify the control circuit and improve the control efficiency. The experimental results show that the thermal EMFs of all the channels are in the range from −11 to 17 nV with the Type A uncertainties varying from 1 to 2 nV. Further experiments indicate that the Allan deviation of the shorted channel of the scanner is less than 10^{-9} V in the sampling time from 10 s to 36 h.**

***Index Terms*— Allan deviation (AD), array driven, relay based, scanner, thermal electromotive force (EMF).**

I. Introduction

LOW thermal electromotive force (EMF) scanner is a precision measurement auxiliary device, which has been widely used in metrology field and testing industry, mainly for the construction of automatic measurement or calibration systems of precision resistor, voltage, and temperature [1]. In principle, the existing low thermal EMF scanners can be divided into two types. For the first type, the low-potential rotating switches of the scanner are driven by stepper motors to realize the channel switching [2], [3]. The second type scanner uses the matching relay as an actuator for channel switching [4]. Due to the influences of the contact material and the working characteristics of the relay, the relay-based scanner cannot catch up the band switch-based scanner in thermal EMF and stability [5]–[7]. In 1999, researchers from Data Proof company and the National Institute of Standard and Technology proposed a guarded scanner using the split-type latching relay in which all the contacts were gold plated. The typical thermal offsets of all the channels of the guarded scanner were less than 20 nV [8]. However, the split-type latching relay is not commercially available, and hence, it is a big challenge to get a metrological scanner with the commercial relays. Up to now, the typical and maximum thermal EMF of an advanced commercial scanner can, respectively, reach 20 and 50 nV with a standard deviation of less than 20 nV [9]–[11]. The relay control circuit in the advanced commercial scanner is mainly made up of two parts. One is the decoding circuit, which is used for converting the serial control signal into the parallel control signal, and the other is the drive circuit, which amplifies the parallel control signal to actuate the relays. In this case, a large number of decoders and drivers are required and the heat disturbance is inevitable. Besides, in each channel of the scanner, the terminals, wires, and solders also have some contributions to the total thermal EMF. Consequently, for a low thermal EMF scanner, a low thermal EMF relay is not enough and it is necessary to seek for some special techniques to obtain an expected low thermal EMF scanner.

A precision resistor load coefficient calibration system was established at the National Institute of Metrology (NIM) in 2012. To realize the batch calibration and get a high efficiency, a multichannel array-driven scanner with low thermal EMF is proposed. The magnetic latching relay (TX2-L2-5V from Panasonic [12]) is selected in the proposed scanner. The contacts of the relay are made of Ag + Au clad material so that the contact potential is as low as nanovolt level and maintains a good stability. Moreover, a pulse current is needed only to actuate the relay, so the heat disturbance coming from the control coils is so small that it can be neglected. Besides, three methods are proposed to further decrease the thermal EMF and improve the stability. First, a terminal selection and matching method is proposed to reduce the thermal EMF caused by the heterogeneity of the terminals. Second, a mechanical connection method is proposed to reduce the contact potential introduced by the solders and wires, and a thermal insulation structure is used to balance the temperature field around the electrical connection points. Third, a power management method is designed to decrease the disturbance caused by the heat effect of the current inside the isothermal box, and thus, it can improve the stability of the scanner. In addition, an array-type control and detection system is proposed to achieve the closed-loop control of the relays. Compared with the existing commercial scanners, the number of the decoders and drivers

Manuscript received October 15, 2015; revised January 8, 2016; accepted January 22, 2016. This work was supported in part by the National Key Scientific Instrument and Equipment Development Project under Grant 2011YQ-090004, in part by the Science and Technology Project of General Administration of Quality Supervision, Inspection and Quarantine, China, under Grant 2014QK237, in part by the Zhejiang Key Discipline of Instrument Science and Technology under Grant JL150526, and in part by the Zhejiang Provincial Key Laboratory of Research for On-Line Testing Equipment Calibration Technology. The Associate Editor coordinating the review process was Dr. V. R. Singh.

L. Qian, Y. Fu, C. Zhang, and L. Chen are with the College of Mechatronics Engineering, China Jiliang University, Hangzhou 310018, China (e-mail: chenlecjlu@163.com).

Z. Li is with the National Institute of Metrology, Beijing 100029, China, and also with the Key Laboratory for the Electrical Quantum Standard, General Administration of Quality Supervision, Inspection and Quarantine, Beijing 100029, China.

Color versions of one or more of the figures in this paper are available online at http://ieeexplore.ieee.org.

Digital Object Identifier 10.1109/TIM.2016.2534278

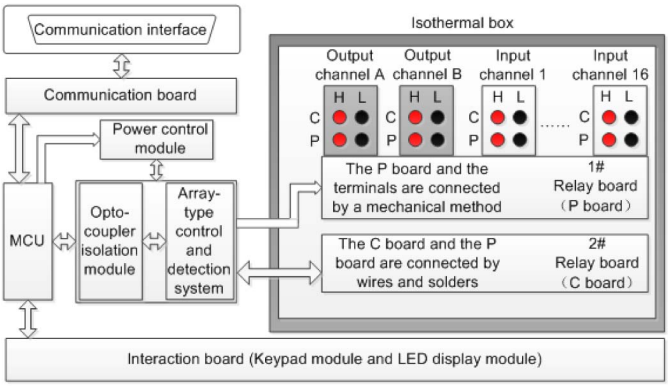

Fig. 1. Functional diagram of the array-driven scanner.

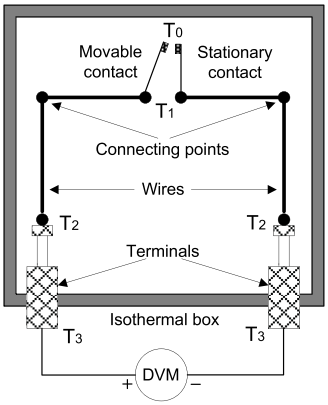

Fig. 2. Simplified model of each channel.

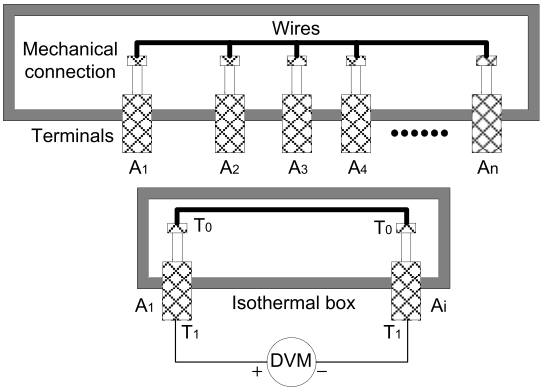

Fig. 3. Structure of the terminal selection and matching method.

is greatly reduced, and the control and detection efficiency is significantly increased. The experimental results indicate that the performance of the proposed scanner is superior to the one without a multichannel array in terms of thermal EMF and stability, especially for Type A uncertainty. The functional diagram of the proposed array-driven scanner is shown in Fig. 1.

II. Thermal EMF Sources

The array-driven scanner is designed for the precision resistor load coefficient calibration system whose main calibration object is the four-terminal resistor. Thus, the thermal EMF mentioned in this paper is limited to the parasitic potential generated at the signal channel between the two potential (P) terminals. Since the contacts of the relay are made of Ag + Au clad material, the terminals are made of gold-plated copper and the wires are made of copper. As a result, the signal channel is composed of different materials. A thermocouple is constituted when the movable contact and stationary contact of the magnetic latching relay are brought into contact (as shown in Fig. 2). Furthermore, the tin–lead solder introduces a number of complex thermocouples. As we know, all the wires and the terminals of the signal channel can be regarded as intermediate conductors with no thermal EMF involved [13] when there is no temperature gradient between the connection points and the signal channel is well symmetric. However, there will be uneven temperature field around the control coils of the relays caused by the working current. Besides, the temperature gradients between the connection points always exist in the actual working conditions due to the disturbance of the power supplies and external environment. In summary, the thermal EMF within one channel is the sum of the parasitic potential produced by each implicit thermocouple [14]. Thus, the methods to reduce the thermal EMF can be concluded to the following three points:

1) minimizing the temperature gradients between the electrical connection points;
2) minimizing the introduction of the third party metal;
3) maximizing the symmetry of the signal channel.

III. Approaches to Reduce the Thermal EMF

Since the thermal EMF reduction strategies can be concluded to three aspects, a combination of several measures can be used in the design to decrease the amplitude of the thermal EMF. These are described in the following sections.

A. Terminal Selection and Matching Method

A terminal selection and matching method is proposed to reduce the thermal EMF caused by the heterogeneity of the terminals. Measurement results of the traditional scanner show that the consistency of the thermal EMFs of different channels cannot be well maintained even the elements and the welding process are exactly the same. The experimental results also prove that the fluctuation of the thermal EMF caused by the heterogeneity of the terminals may even be up to 100 nV. In order to solve this problem, a terminal selection and matching method is proposed. As shown in Fig. 3, terminal A_1 is randomly selected as a benchmark and all the remaining terminals (A_2–A_n) are shorted with A_1 in proper order by a mechanical method. In order to simulate the actual working state, all the terminals are installed on a simplified isothermal box. All the electrical connection points of the terminals are located inside the box. The temperature inside the simplified isothermal box is defined as T_0 and the external temperature is defined as T_1. Moreover, the detection polarity reversal method mentioned in Section V is adopted to calculate the thermal EMFs of different pairs of terminals. To eliminate the disturbance from the heat effect, a delay of 60 s is needed after the manual wiring during the measurement process. After testing all the terminals, we can get

$$E_{A_1A_2}(T_1, T_0), E_{A_1A_3}(T_1, T_0) \ldots E_{A_1A_n}(T_1, T_0). \quad (1)$$

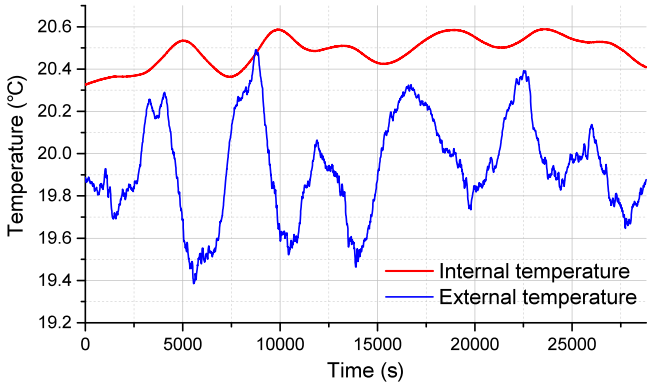

Fig. 4. Change curves of (a) internal temperature and (b) external temperature of the scanner for 8 h.

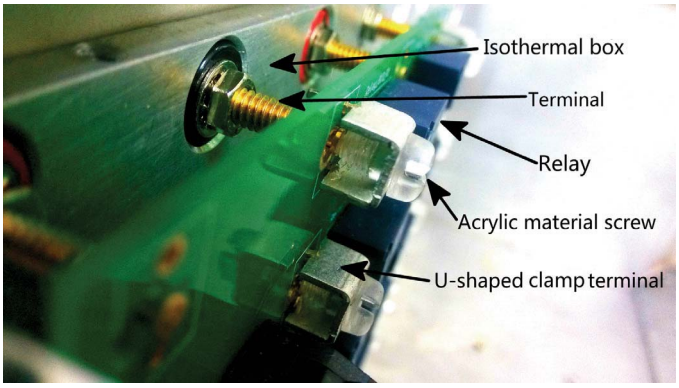

Fig. 5. Detailed view of the thermal insulation structure and the mechanical connection method: isothermal box, terminal, relay, acrylic material screw, and U-shaped clamp terminal can be seen.

As

$$E_{A_iA_j}(T_1, T_0) = E_{A_1A_j}(T_1, T_0) - E_{A_1A_i}(T_1, T_0) \ldots, 1 < i, j \leq n. \quad (2)$$

If

$$E_{A_1A_i}(T_1, T_0) = E_{A_1A_j}(T_1, T_0). \quad (3)$$

Then

$$E_{A_iA_j}(T_1, T_0) = 0. \quad (4)$$

In this case, A_i and A_j are the ideal paired combination. Finally, all the obtained measurement results are sorted in the ascending way and most terminals can be matched except a few nonideal ones.

B. Thermal Insulation Structure and Mechanical Connection Method

A thermal insulation structure is used to balance the temperature field around the electrical connection points, and thus, it can reduce the thermoelectric potential in the channel. An isothermal box is mounted inside the scanner to enclose all the relays and electrical connection points. A layer of high-density sponge is also attached around the isothermal box for further heat insulation. Two temperature sensors were put inside and outside of the scanner, respectively. Measurement results (Fig. 4) show that the variation of the internal temperature can track the external one and the attenuation coefficient is about 1/5 in a lag time about 30 min. Therefore, a conclusion can be obtained that the thermal time constant of the box is Tc $= -30$ min/ln $(1 - 1/5) = 134$ min.

In the traditional scanner, a number of complex thermocouples are involved because the terminals and the relay boards are connected by the wires and the solders. Consequently, a mechanical connection method is proposed to reduce the contact potential introduced by the wires and the solders. As shown in Fig. 5, the electrical connection point of the terminal is tightly clamped on the relay board by an acrylic material screw after passing through a microphone-shaped pad. The U-shaped clamp terminal fixed in the relay board provides the screw with the required support force. With the mechanical connection method, the number of the electrical connection points in the signal channel is decreased with no solder involved. In this way, the overall thermal EMF can be greatly reduced.

C. Power Management Method and Optocoupler Isolation Module

An independent power supply module is designed for the low thermal EMF scanner. Since the power of the array-type control and detection system will be cutoff once the channel is successfully switched, the disturbance caused by the heat effect of the current in the isothermal box can be decreased as much as possible. Moreover, the main controller and the array-type control and detection system are isolated by the optocoupler isolation module, which enhances the anti-interference ability of the key modules and ensures the accuracy of signal transmission.

IV. Array-Type Control and Detection System for Relays

The adopted relay has two pairs of switch contacts with synchronous action. One is used to change the electrical signal of the input terminals and the other is used for indicating the current state of the relay. Meanwhile, the closing and clearing actions of the contacts are controlled by two individual coils.

An array-type control system is developed to effectively simplify the control circuit, improve the control efficiency, and reduce the introduction of the thermal effects. In the traditional scanner, the utilization rate of the relay drivers is not so high. A total of 64 drivers and their corresponding decoders are needed to control 128 relays. Therefore, the number of the chips in control circuit is considerable and the introduced thermal disturbance is inevitable. With the array-type control system, only 16 drivers are needed and no decoders involved to control the same number of relays. As shown in Fig. 6, the closing control coils of the four relays in one channel form a coil cell and the four clearing control coils form another one. Thus, every four relays contain two cells. Note that each coil is connected with a diode before parallel connected so as to prevent the reflux of the control signal. As a consequence, all the 128 relays in the array contain 64 cells, which are arranged in a matrix of eight rows by eight columns.

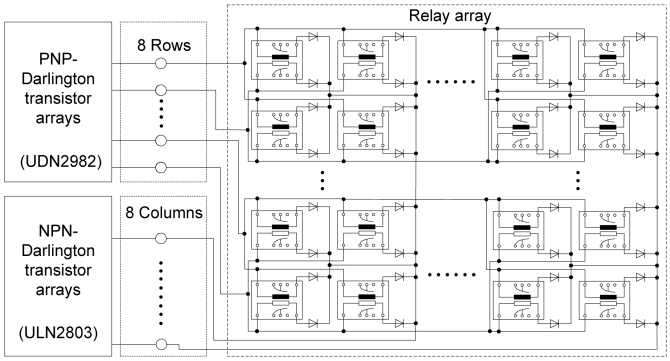

Fig. 6. Details of the array-type control system for relays. The relay array consists of 128 relays, and only a part of them are shown here. The black rectangle and the white rectangle inside the relay model represent the two control coils.

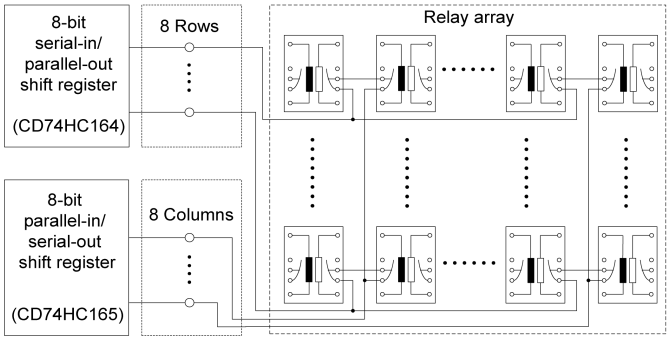

Fig. 7. Details of the array-type detection system for relays. The relay array consists of 128 relays, and only a part of them are shown here.

The eight-row control terminals and the eight-column control terminals are connected to PNP- and NPN-type drivers, respectively. Thus, every cell can be controlled by properly combining the row control signals and the column control signals.

To make sure that the scanner is working as expected, an array-type detection system depending on progressive scan is designed to detect the real-time states of all the relays. The LED lights are used to indicate the current states of the relays in the traditional scanner. Since the states of the relays are monitored by manual method, it is very inconvenient to identify the relay failures, especially in the remote control. The array-type detection system can be a good solution to solve the problem. The current states of all the relays are feedback to the main controller by means of progressive scan in the array-driven scanner. As shown in Fig. 7, the undetected contacts of two relays form a contact cell by a series connection. Thus, every four relays in one channel contain two cells. The two cells are set up in one channel to narrow the scope of inspection when some relays are invalid. All the 64 cells are arranged in a matrix of eight rows by eight columns. During the detecting process, the scan signal generated by the controller enters the row detection terminals of the relay array after an 8-bit serial-in/parallel-out shift register. Logic level 0 or 1 will be generated at the corresponding column detection terminals and all the detection results will be fed back to the controller through the 8-bit

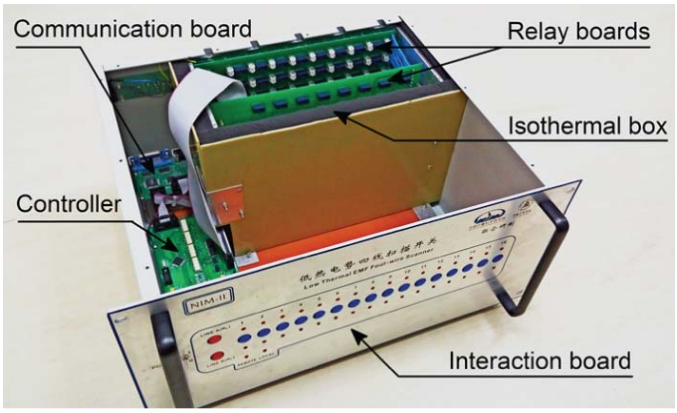

Fig. 8. Overview of the scanner: communication board, controller, interaction board, relay boards, and isothermal box are visible.

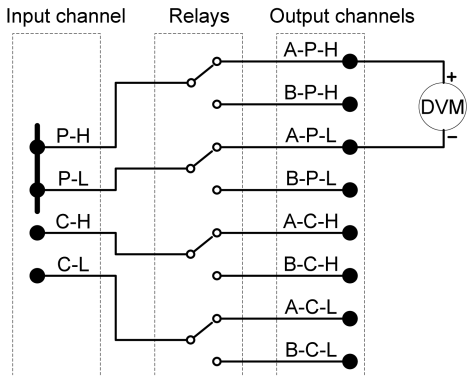

Fig. 9. Thermal EMF measurement structure for scanner. P: potential terminals. C: current terminals. H: high terminal. L: low terminal. A: output channel A. B: output channel B.

parallel-in/serial-out shift register. A correct detection result will be accepted if the four relays in the selected channel have closed simultaneously. According to the detection results, the system will automatically judge whether all the relay actions are working correctly.

In this way, the closed-loop control of relays is achieved to ensure the accuracy of channel switching. The internal structure of the scanner is shown in Fig. 8.

V. Evaluation and Analysis

The thermal EMF was measured by an Agilent 34420A digital voltmeter (DVM), which was configured with a 1-mV range and ten power line cycles to get the $6(1/2)$ digits resolution with filter OFF. All experiments were carried out in a shielded room at the NIM. The temperature of the shielded room was set at 20 °C with a stability of ±0.5 °C. The measurement setup is shown in Fig. 9. All the input P terminals of the scanner were shorted together, and the output P terminals of channel A or B were connected to the high and low polarity terminals of the ch1 of the DVM, respectively. The detection polarity reversal method was adopted to calculate the thermal EMF to eliminate the offset voltage introduced by the DVM and overcome the asymmetry in the reading between the positive and negative polarity positions [6], [15]. The measuring steps are as follows: 1) V_{+1} was measured at

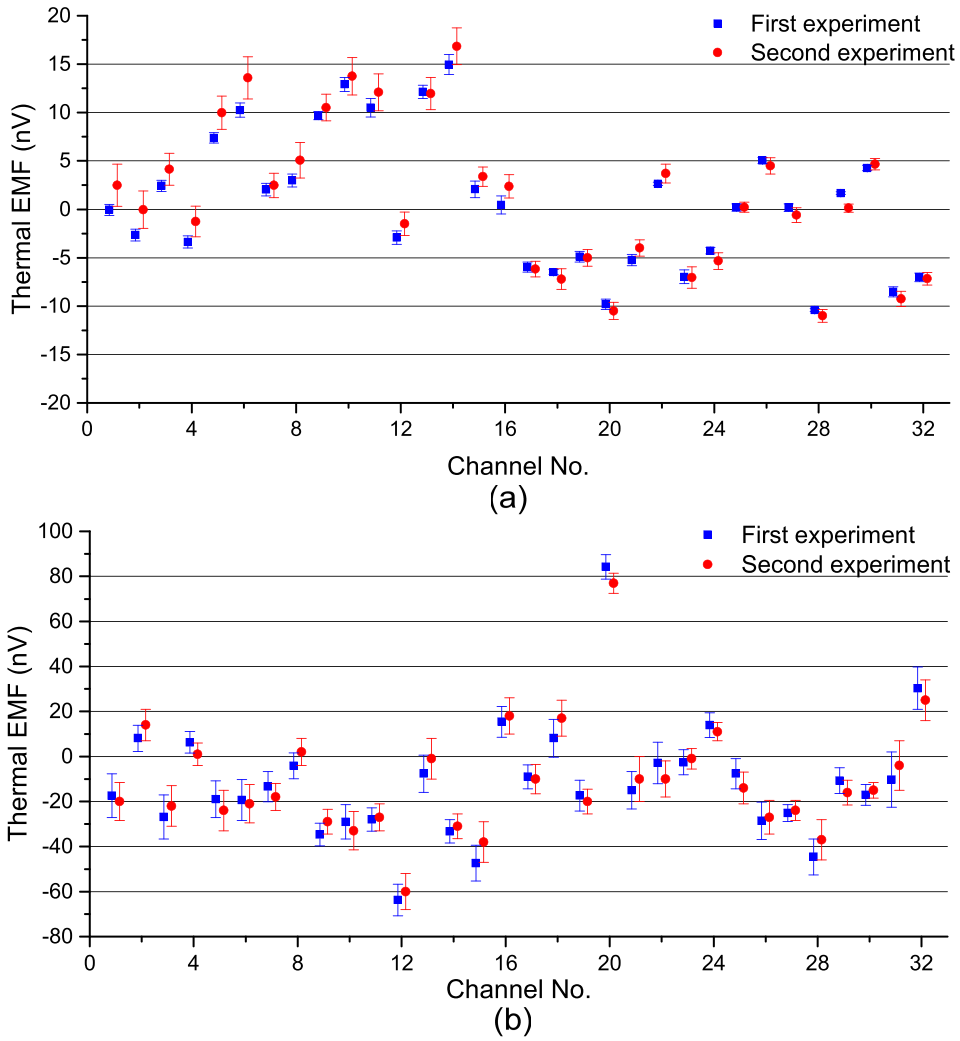

Fig. 10. Measured thermal EMFs of the 32 outputs of (a) array-driven scanner and (b) NIM-I scanner. Channel Nos. 1–16: channels A1–A16. Channel Nos. 17–32: channels B1–B16. Blue squares: mean value of five consecutive measurements in the first experiment. Red disks: mean value of five consecutive measurements obtained by repeating the first experiment after five days. Uncertainty bars: Type A uncertainty (standard deviation of the mean at $k = 1$).

the normal polarity for 25 s; 2) V_{-1} and V_{-2} were measured at the later reverse polarity for 50 s; and 3) another 25 s at the normal polarity again to get V_{+2}. The average value in every 25 s was printed as the single measurement result to reduce the typical noise introduced by the input cables of the DVM. Finally, the EMF can be determined by the following equation:

$$U = ((V_{+1} + V_{+2})/2 - (V_{-1} + V_{-2})/2)/2. \tag{5}$$

Notably, additional time is needed to eliminate the disturbance from the heat effect of the channel switching and the manual wiring. A delay of 5 s after channel switching and a delay of 60 s after manual wiring were set before the data acquisition process in the measurement software.

A. Analysis of the Repeatability Measurement Results

Experiments have been carried out to evaluate the performance of the repeatability of each channel. The thermal EMFs of the scanner were measured in the method of repeating five times a scan of one measure over the 32 channels. The results of the first experiment [Fig. 10(a)] show the mean value of the five consecutive measurements with an associated Type A uncertainty (standard deviation of the mean at $k = 1$). It shows that the thermal EMFs of all the channels never exceed 20 nV with the Type A uncertainties below 1 nV. To evaluate the stability and repeatability of the scanner, the same experiment was repeated after five days. It shows a similar result as the previous one. The thermal EMFs of all the 32 channels range from −11 to 17 nV with the Type A uncertainties varying from 1 to 2 nV. Comparing the results of the two experiments, it can be found that the whole distributions of the thermal EMFs of the two experiments are approximately the same. The tiny variations of the mean value and the standard deviation at the nanovolt level can be attributed to the slight changes of the external environment. It is a normal phenomenon for the relay-based scanner.

To compare the thermal EMF and stability of the scanners with and without the multichannel array, a scanner (NIM-I) was chosen as the compared object. The NIM-I scanner is the previous version of the array-driven scanner and it refers to the traditional design method of the mainstream commercial scanner. The same commercial relays, the same

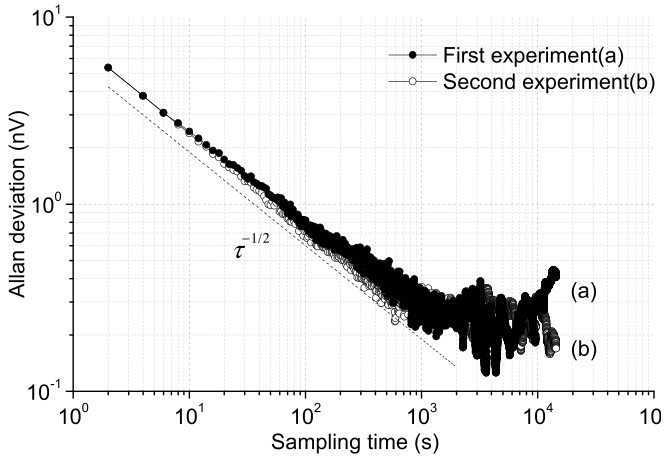

Fig. 11. AD versus sampling time for the shorted DVM in (a) and (b) two independent experiments with the DVM in filter OFF condition.

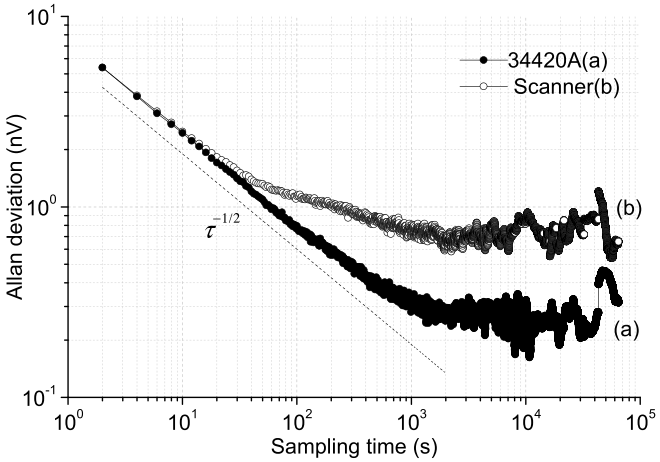

Fig. 12. AD versus sampling time for the (a) shorted DVM and the (b) output channel A of the input shorted scanner with the DVM in filter OFF condition.

terminals, and the same processing technology were adopted in the array-driven scanner and the NIM-I scanner. However, the NIM-I scanner does not have the multichannel array. In order to compare the two scanners intuitively, the same experiments were carried out to evaluate the thermal EMF and stability of the NIM-I scanner. The results [Fig. 10(b)] indicate that the thermal EMFs of all the channels are in the range from -65 to 30 nV except the channel B4, and the Type A uncertainties range from 4 to 12 nV. Comparing the array-driven scanner with the NIM-I scanner, the performance of the array-driven scanner is superior to the NIM-I scanner in terms of thermal EMF and stability, especially for Type A uncertainty.

B. Analysis of the Stability in Continuous Measurement

Since the load coefficient calibration process of the precision resistor usually takes a very long time, it is necessary to study the stability of the scanner in the continuous measurement. Fig. 11 shows two log–log plots of the Allan deviation (AD) (square root of the Allan variance [16]) for the shorted DVM in two independent experiments, which, respectively, contains a series of 14 400 points acquired in 8 h with a sampling period of 2 s. Fig. 11(a) shows that the AD varies as $\tau^{-1/2}$ within sampling time τ from 2 to 500 s, which corresponds to the white noise introduced by the DVM [17]. The $1/f$ noise floor of 0.27 nV is achieved at the sampling time longer than 500 s. After the time point $\tau \approx 3200$ s, AD is influenced by a period perturbation, which can be attributed to the temperature fluctuation in the laboratory. Notably, the AD at τ_0 (2 s) in the first experiment (5.367 nV), caused by the typical noise between the two input cables of the DVM, is consistent with the data in the datasheet of the 34420A [18]. The same experiment was repeated after two days. It shows that the AD of Fig. 11(b) is nearly identical to that of Fig. 11(a), which indicates that the tiny changes of the external environment do not affect the stability of the DVM in the long-term measurement.

Fig. 12 shows the AD of the shorted DVM and the output channel A of the input shorted scanner in 36 h. It shows that the corresponding values of Fig. 12(a) and (b) are almost the same from 2 to 40 s, which demonstrates that the white noise in the scanner measurement mainly originates from the DVM. After the time point $\tau \approx 40$ s, the values of Fig. 12(b) are bigger than those of Fig. 12(a), which means that the noise introduced by the scanner is gradually emerging. Finally, the $1/f$ noise introduced by the DVM is maintained at 0.27 nV and the $1/f$ noise caused by the DVM and the scanner is maintained at 0.58 nV at the sampling time longer than 2000 s. The sudden change of AD around $\tau \approx 43\,200$ s in the two experiments can be attributed to some disturbances in the lab, which cannot be predicted.

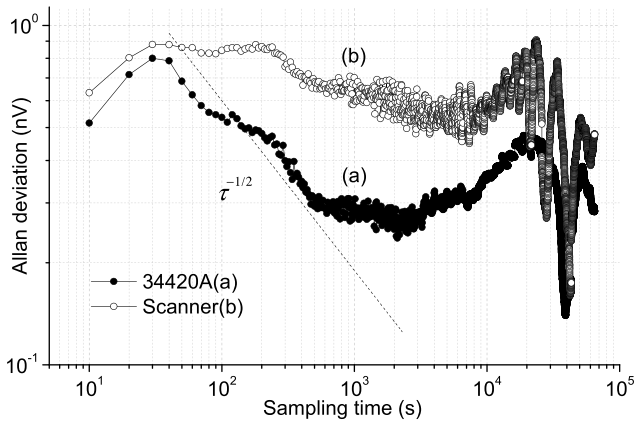

Fig. 13. AD versus sampling time for the (a) shorted DVM and the (b) output channel A of the input shorted scanner with the DVM in filter ON condition.

In order to evaluate the stability of the scanner, another repeat experiment was conducted with the DVM configured with filter ON and the τ_0 is 10 s. The experimental results (Fig. 13) indicate that the ADs of both experiments increase with the sampling time below 30 s. This is because the digital filter function of the DVM slows down its own measurement rate and the sampling frequency is too high [19]. As the digital filter function of the DVM has averaged the white noise, the AD does not vary as $\tau^{-1/2}$ anymore within the sampling time from 30 to 500 s. However, we can still draw the conclusion that the AD of the scanner is less than 10^{-9} V in the sampling time from 10 s to 36 h.

VI. Conclusion

The disadvantages of the relay in terms of the thermal EMF and stability can be overcome by three novel improvements proposed in this paper. The evaluation results show that the thermal EMFs of all the channels range from −11 to 17 nV with the Type A uncertainties ranging from 1 to 2 nV. Moreover, the closed-loop control of the relays is realized with an array-type control and detection system, which greatly improves the efficiency of channel switching. Therefore, the overall performance of the array-driven scanner is better than the band switch-based scanner. It can be applied in most precision measurement systems and can also satisfy most calibration purpose. Its long-term reliability and repeatability will be studied in the future.

Acknowledgment

The authors would like to thank K. Wang for his help with experimental data collection and Y. Bai, Z. Fu, N. Wang, and G. Wang for their valuable discussions. The authors would also like to thank the reviewers and the Editors for their valuable suggestions to improve this paper.

References

[1] A. Sosso and R. Cerri, "Practical scanner for voltage metrology," in *IEEE Conf. Precis. Electromagn. Meas. Dig. (CPEM)*, Jun. 2008, pp. 234–235.

[2] Y. Sakamoto, A. Odawara, and T. Endo, "Computer-controlled low thermal EMF rotary switch," *IEEE Trans. Instrum. Meas.*, vol. 40, no. 2, pp. 337–339, Apr. 1991.

[3] Y. Sakamoto, A. Odawara, and T. Endo, "Computer-controlled low thermal EMF rotary switches (voltage measurement)," in *IEEE Conf. Precis. Electromagn. Meas. Dig. (CPEM)*, Jun. 1990, pp. 126–127.

[4] J. A. Marshall, T. A. Marshall, D. G. Jarrett, and R. F. Dziuba, "A low thermal guarded scanner for high resistance measurement systems," in *IEEE Conf. Precis. Electromagn. Meas. Dig. (CPEM)*, Jun. 1996, pp. 20–21.

[5] R. Chayramy and S. Solve, "A very low thermal EMFs computer-controlled scanner," in *IEEE Conf. Precis. Electromagn. Meas. Dig. (CPEM)*, Jul. 2012, pp. 548–549.

[6] R. Chayramy and S. Solve, "A very low thermal EMF computer-controlled scanner," *Meas. Sci. Technol.*, vol. 24, no. 2, p. 025008, 2013.

[7] K. Inagaki *et al.*, "EMF migration between Shapiro steps on PbInAu/oxide/PbAu junctions under constant current biases," in *IEEE Conf. Precis. Electromagn. Meas. Dig. (CPEM)*, Jun. 1990, pp. 108–109.

[8] D. G. Jarrett, J. A. Marshall, T. A. Marshall, and R. F. Dziuba, "Design and evaluation of a low thermal electromotive force guarded scanner for resistance measurements," *Rev. Sci. Instrum.*, vol. 70, no. 6, pp. 2866–2871, 1992.

[9] Guildline Instruments Limited. (Oct. 2008). *8 and 16-Channel Low Thermal Quad Scanners*. [Online]. Available: http://www.guildline.com/Datasheet/guildline6664BDatasheet.pdf.

[10] Measurements International Limited. (Mar. 2012). *Automated Low Thermal Matrix Scanners*. [Online]. Available: http://www.mintl.com/media/pdfs/4200-series.pdf.

[11] Data Proof. *Low Thermal Guarded Scanner*. [Online]. Available: http://www.dataproof.com/opt3_data_sheet_wwwdataproof.htm.

[12] Panasonic Electric Works Europe AG. *TX Relays*. [Online]. Available: https://www.panasonic-electric-works.com/cps/rde/xbcr/pew_eu_en/ds_61022_en_tx.pdf.

[13] G. Grängsjö, J. Sandblom, H. R. Ulfendahl, and M. Wolgast, "Theory of the heated thermocouple principle," *Acta Physiol. Scandin.*, vol. 66, no. 3, pp. 366–373, 1966.

[14] A. D. Wilson and H. B. Ulsh, "Theory of the parallel thermocouple," *Rev. Sci. Instrum.*, vol. 39, no. 3, pp. 346–348, 1968.

[15] S. K. Jaiswal, "Complete characterization of a low thermal scanner for automatic voltage measurement," *MAPAN-J. Metrol. Soc. India*, vol. 23, no. 1, pp. 31–38, 2008.

[16] J. E. Gray and D. W. Allan, "A method for estimating the frequency stability of an individual oscillator," in *Proc. IEEE 28th Annu. Symp. Freq. Control*, May 1974, pp. 243–246.

[17] T. J. Witt, "Allan variances and spectral densities for DC voltage measurements with polarity reversals," *IEEE Trans. Instrum. Meas.*, vol. 54, no. 2, pp. 550–553, Apr. 2005.

[18] Keysight Technologies. (Mar. 2003). *Keysight 34420A Nano Volt/Micro Ohm Meter*. [Online]. Available: http://literature.cdn.keysight.com/litweb/pdf/34420-90001.pdf?id=1000003601:epsg:dow.

[19] T. J. Witt, "Using the Allan variance and power spectral density to characterize DC nanovoltmeters," in *IEEE Conf. Precis. Electromagn. Meas. Dig. (CPEM)*, Apr. 2000, pp. 667–668.

[20] T. J. Witt, "Using the Allan variance and power spectral density to characterize DC nanovoltmeters," *IEEE Trans. Instrum. Meas.*, vol. 50, no. 2, pp. 667–668, Apr. 2001.

Lushuai Qian was born in Zhejiang, China, in 1993. He received the B.S. degree in automation from China Jiliang University, Hangzhou, China, in 2014, where he is currently pursuing the M.S. degree in detection technology and automation equipment.

His current research interests include electrical measurement technology and instrumentation.

Yaqiong Fu was born in Hebei, China, in 1983. He received the M.S. degree from China Jiliang University (CJLU), Hangzhou, China, in 2009.

He joined the College of Mechatronics Engineering, CJLU, in 2009. His current research interests include modern precise electromagnetic measurement and instrument technology.

Zhengkun Li was born in Henan, China, in 1977. He received the Ph.D. degree in electrical and electronic engineering from Xi'an Jiaotong University, Xi'an, China, in 2006.

He joined the Quantum Division, National Institute of Metrology, Beijing, China, in 2002. He is currently involved in research on quantum mass standard (joule balance).

Cunkai Zhang was born in Hebei, China, in 1990. He received the B.S. degree in automation from Northeastern University at Qinhuangdao, Qinhuangdao, China, in 2013. He is currently pursuing the M.S. degree with the College of Mechatronics Engineering, China Jiliang University, Hangzhou, China.

His current research interests include electrical measurement technology and instrumentation.

Le Chen was born in Zhejiang, China, in 1959. She received the Ph.D. degree from Zhejiang University, Hangzhou, China, in 2006.

She is currently a Professor with the College of Mechatronics Engineering, China Jiliang University, Hangzhou. Her current research interests include modern precise electromagnetic measurement and instrument technology.